

Multimode Interference Biosensor Working With Multiple Wavelengths And Two Polarizations

Moisi Xhoxhi, Partizan Malkaj, Tatjana Mulaj, Alma Dudia, Aurel Ymeti

Abstract: In this paper is presented a new design for Young Interferometer (YI) biosensor and the analysis of output power of a MMI waveguide that will be used in it. The waveguides are simulated with OptiBPM software, which is a Waveguide Optics Modeling software from Optiwave Corporation. Output power and excess loss is analysed for 1×5 and 1×10 planar MMI waveguides for different wavelengths with TE and TM polarization. It is demonstrated that output power decreases exponentially with the increase of the wavelength for both polarizations. The evaluation of the excess loss shows that it is higher for a TM polarized field for all the wavelengths and periodicities considered. Power imbalance seems to have small values suggesting the use of MMI waveguides as good power splitters. A comparison of the excess loss between 1×5 and 1×10 MMI waveguides shows that it remains almost the same for both polarizations for the optimum wavelength ($\lambda = 647$ nm).

Index Terms: biosensor, integrated optics, MMI structures, waveguides, multichannel interferometer, multiple wavelength, two polarizations, virus detection

1 INTRODUCTION

BIOSENSORS are a new technology in medical diagnostics that have had a big impact and have accelerated the investigation in many research fields where the most important is biomedical analysis. They are used to detect and measure the presence of a specific analyte (microorganism or chemical substance that is subject to analysis) in a specific sample (blood, serum, beverage etc) by means of a recognition system. Hundreds of different biosensors exist nowadays depending on their design and working principle. Most of the research in this field until now has been focused on improving their sensitivity, selectivity, and stability, while little research is done to reduce their high cost of production and increase their measurement capacity. In this paper is presented a new design for the integrated optics Young Interferometer (YI)[1] that addresses the two latter issues. The original biosensor, as shown in Fig. 1, is based on Young's Interferometer (YI) and combines the optical output from four channels to form interference fringes on a CCD camera.

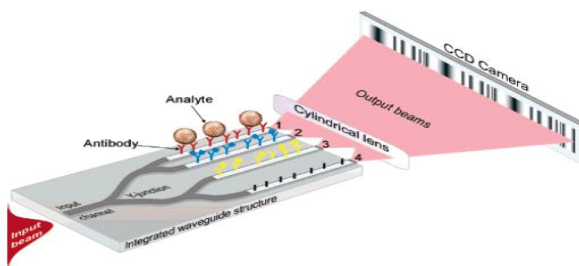


Fig. 1. Schematic representation of the four-channel integrated optical YI biosensor: 1, 2 and 3 indicate the measuring channels, and 4 is the reference channel. Adapted from "Fast, Ultrasensitive virus detection using a Young Interferometer sensor" by A. Ymeti et al., 2007, Nano Letters, 7, p. 394-397. Copyright 2007 by the American Chemical Society.

excellent properties as compact size, low loss and large fabrication tolerances [4] they are suitable to be used in biosensors and bioassays to reduce their cost. The main component of the new design is the first MMI waveguide, shown in Fig. 4, which is the subject of our analysis. The thickness of the core layer, height of the channel ridge, thickness of the substrate and cover layer are the same as the Young Interferometer [1]. Table 1 presents all the parameters for the first MMI waveguide. We report on the output power and excess loss when changing different parameters such as wavelength, polarization and periodicity of replicas of the first MMI waveguide because it directly affects the quality of measurements in the biosensor. Fabrication tolerances are independent from the number of output channels, N , but are proportional to the output channel separation [2]. Therefore, when increasing the number of output channels, we expect less fabrication tolerances. Standard splitters based on X- and Y- junction design suffer from high reflection and radiation losses due to branching complexity [3]. On the other hand, there has been a growing interest in the application of the multimode interference (MMI) waveguides in integrated optics [4], [5], due to their excellent properties and ease of fabrication. They are quite easy to design and are compatible with both weakly guided and strongly guided structures [5].

Sensing is accomplished by measuring the shift in phase of the output beams due to the changes in the binding surface. The new design that we propose is composed of two MMI waveguides one after another, as shown in Fig. 2b. This design offers more output channels for simultaneous measurements, in this way increasing its measurement capacity. Because MMI waveguides have

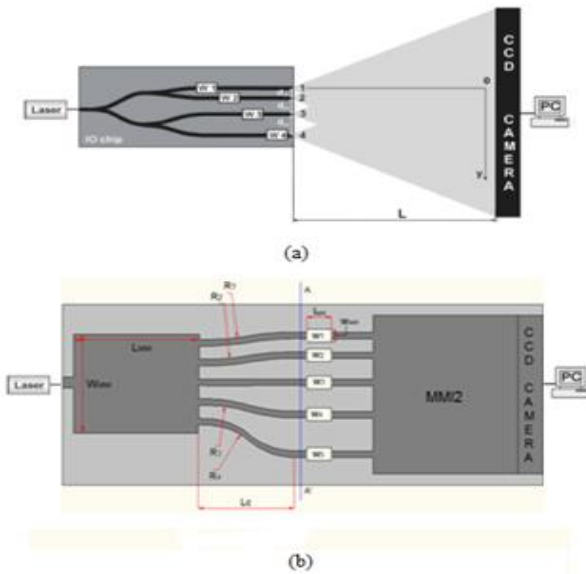


Fig. 2. (a) Layout of the original four-channel YI biosensor. Adapted from "Development of a Multichannel Integrated Young Interferometer Immunosensor" by A.Ymeti,2004, ISBN 90-365-2028-2. (b) The new design of the biosensor with two MMI waveguides based on symmetric interference.

2 MMI PRINCIPLE AND DESIGN

The multimode interference (MMI) effect in multimode waveguides is caused due to the reflecting of the input field in the side walls of the waveguide. This causes a weighted combination of even and odd lateral modes inside the multimode region, which recombine and form single or multiple images of the input field at periodic intervals [4], as shown in Fig. 3. These images can then be coupled to single-mode waveguides at the end of the multimode region to form N×N or 1×N splitters or cross-couplers. The 1×N beam splitters, which are used in the new biosensor design, are obtained by center-feeding the multimode waveguide with a symmetric field profile [4]. In this case, only the even modes are excited in the multimode region and the length of the MMI waveguide will be 4-times shorter if we used general interference [6]. The imaging is obtained by linear combination of the even (symmetrical) modes, and this type of MMI mechanism is called symmetric interference [4].

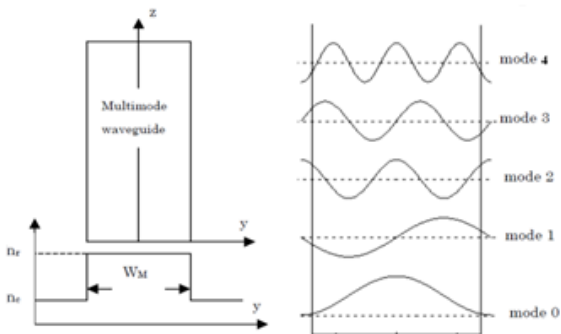


Fig. 3. Step-index multimode waveguide, refractive index distribution and lateral field profiles of the first 5-guided modes. Adapted from "Multimode interference couplers design and applications" by L. B. Soldano, 1994, Delft University Press. Copyright 1994 by L. B. Soldano.

According to the symmetric interference mechanism, the single images of the input field will be obtained at the multimode section length, L , defined by (1) [4]:

$$L = p \left(\frac{3L\pi}{4} \right) \text{ with } p = 0,1,2 \dots, \tag{1}$$

while the N -fold images are obtained at

$$L = \frac{p}{N} \left(\frac{3L\pi}{4} \right) = \frac{p}{N} \frac{n_c W_e^2}{\lambda} \tag{2}$$

where L_π , known as the beat length, is defined by

$$L_\pi \approx \frac{\pi}{\beta_0 - \beta_1} = \frac{4n_c W_e^2}{3\lambda} \tag{3}$$

Here, β_0 and β_1 are propagation constants of the fundamental and the first-order lateral modes, respectively, λ is the free space wavelength, n_c is the effective index of the waveguide core, p is the periodicity of replicas, N is the number of output channels and W_e is the effective width of the multimode waveguide. We can approximate the effective width, W_e , of the MMI area as:

$$W_e \approx W + \frac{\lambda}{\pi} \frac{\left(\frac{n_{cl}}{n_c} \right)^{2\sigma}}{\sqrt{n_c^2 - n_{cl}^2}} \tag{4}$$

where W is the physical width of the MMI area and n_{cl} is the effective cladding index of the MMI waveguide, and integer $\sigma = 0$ for TE modes and $\sigma = 1$ for TM modes [4]. For strongly guided waveguides we get $W_e \approx W$ [2]. Due to the different values of the integer σ , there is a difference of the MMI optimal length between TE and TM modes.

3 SIMULATION OF THE FIRST MMI WAVEGUIDE WITH 5 OUTPUT CHANNELS

In our design we consider a MMI splitter based on a ridge structure. Fig. 4 shows a 2D and 3D view of the first MMI waveguide used in the new design, while Table 1 presents the related parameters.

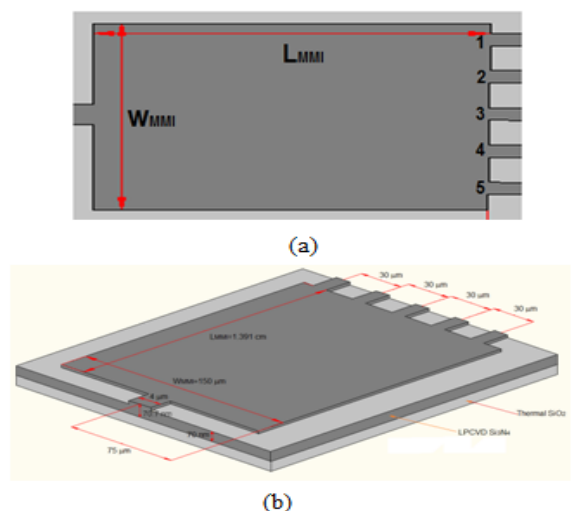


Fig. 4. a) Schematic 2D view of the first MMI b) Schematic 3D view of the first MMI

TABLE 1 PARAMETERS OF THE FIRST MMI WAVEGUIDE WITH 5 OUTPUT CHANNELS

Name	Symbol	Value	Dimension
Width of first MMI	W_{MMI}	150	μm
Thickness of the core layer	d_{F2}	70	nm
Height of the channel ridge	h_1	0.7	nm
Thickness of the SiO2 subs layer	d_s	1.25	μm
Thickness of the SiO2 cover layer	d_c	1.5	μm
Effective core index	n_c	2.0	-
Effective cladding index	n_{cl}	1.45	-
Number of output channels	N	5	-
Channel width	W	4	μm
Interdistance between the output channels	l_{int}	30	μm
Length of first MMI	L_{MMI}	1.391	cm

The wavelengths used in these simulations are:

- $\lambda_1 = 0.647 \mu\text{m}$
- $\lambda_2 = 2\lambda_1 = 1.294 \mu\text{m}$
- $\lambda_3 = 3\lambda_1 = 1.941 \mu\text{m}$
- $\lambda_4 = 2\lambda_2 = 4\lambda_1 = 2.588 \mu\text{m}$

These wavelengths fulfill the condition that for each of them we can have the same number of output replicas without changing the other parameters of the waveguide. The length of MMI waveguide presented in table 1 is calculated from (2) in order to take first periodicity ($p = 1$) for λ_1 . Equation (2) implies that by maintaining constant the width and length of MMI waveguide, we will take the second, third and fourth periodicity for the output replicas for λ_2 , λ_3 and λ_4 , respectively.

3.1 Analysis of Output Power for TE Polarized Input Field

This section analyzes output power taken from the simulation of the waveguide in Fig. 4. using TE polarized Gaussian input field. Table 2 shows the wavelengths and the respective period of the replicas in the output channels for this waveguide.

TABLE 2 PERIOD OF REPLICAS AND THE RESPECTIVE WAVELENGTH

Length of MMI waveguide ($L_{MMI} = 13.91 \text{ mm}$)				
Period (p)	1	2	3	4
Wavelength (λ) μm	0.647	1.294	1.941	2.588

Fig. 5. shows the relationship between output power in channel 1 versus wavelength. Also, in this figure is shown the fitting exponential function of the form $y = a \cdot \exp(bx)$ and the corresponding correlation coefficient R . The high value of the correlation coefficient implies that output power in channel 1 decreases exponentially with the increase of the wavelength.

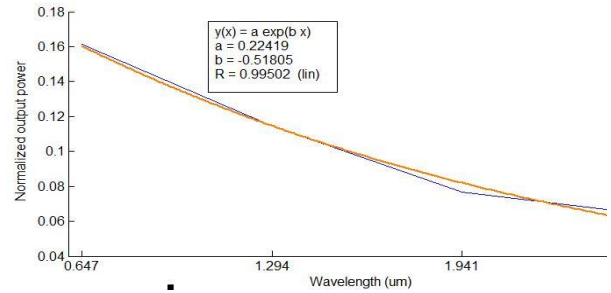


Fig. 5. Power output in channel 1 vs. Wavelength

Fig. 6. shows the same relationship between output power and the wavelength used in the simulations for the other channels of the waveguide. Again, we can see that for each of the 5 channels output power decreases exponentially with wavelength. Table 3 shows the parameters a and b of the fitting exponential functions, of the form $y = a \cdot \exp(bx)$, for each curve and the corresponding correlation coefficients R .

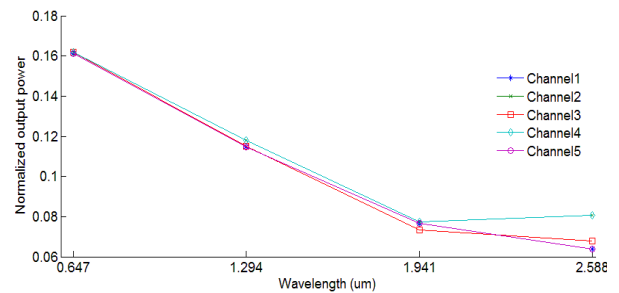


Fig. 6. Output power vs. Wavelength for all the channels of the first MMI waveguide

Channel	a	b	R
1	0.22419	-0.51805	0.99502
2	0.21046	-0.43574	0.96577
3	0.22835	-0.53726	0.99308
4	0.21046	-0.43574	0.96577
5	0.22419	-0.51805	0.99502

The correlation coefficient's values in Table 3 move in the range 96.5% - 99.5%, which insinuate an exponential decay of the output power in all the channels of the MMI waveguide with the increase of the wavelength. Fig. 7. shows the field distribution in the multimode section of the waveguide for the 4 different wavelengths considered in these simulations. In these figures we can observe a greater dispersion of the field for higher wavelengths (higher periodicities). Due to the increase of dispersion, the replicas become less accurate and their coupling with the output channels less effective. This causes the reduction of the output power with the increase of the wavelength used. The same thing is observed in Fig. 8., which shows a 3D view of the field distribution in the multimode section of the waveguide.

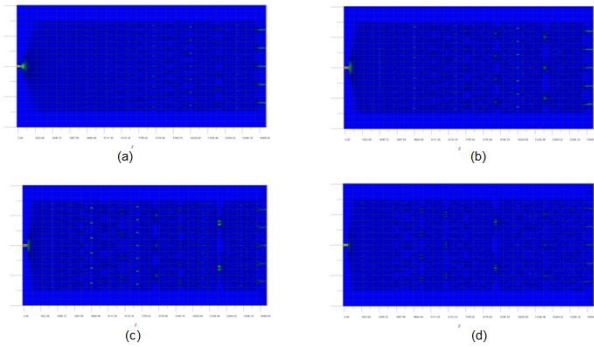


Fig. 7. Field distribution for TE polarized field inside the MMI waveguide: (a) $\lambda_1 = 0.647 \mu\text{m}$ (first periodic interval) , (b) $\lambda_2 = 1.294 \mu\text{m}$ (second periodic interval), (c) $\lambda_3 = 1.941 \mu\text{m}$ (third periodic interval), (d) $\lambda_4 = 2.588 \mu\text{m}$ (fourth periodic interval)

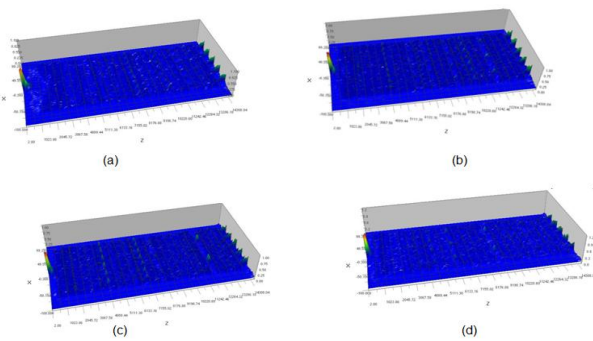


Fig. 8. 3-D view of the field distribution for a TE polarized field inside the MMI waveguide: (a) $\lambda_1 = 0.647 \mu\text{m}$ (first periodic interval) , (b) $\lambda_2 = 1.294 \mu\text{m}$ (second periodic interval), (c) $\lambda_3 = 1.941 \mu\text{m}$ (third periodic interval), (d) $\lambda_4 = 2.588 \mu\text{m}$ (fourth periodic interval)

3.2 Analysis of output power for TM polarized input field

This section analyzes output power of the same MMI waveguide for a TM polarized input field with a Gaussian profile. The relationship between the output power for each channel versus wavelength, shown in figure 9, is similar to TE polarization. This is approved by the high values of the correlation coefficients for the exponential fitting functions shown in Table 4. Therefore, even for TM polarized input field there is an exponential decrease of output power with the increase of the wavelength.

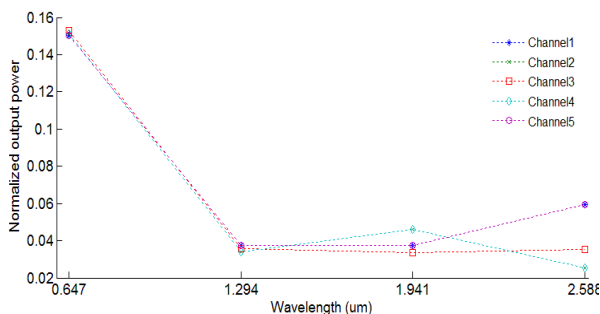


Fig. 9. Output power vs. Wavelength for TM polarization

TABLE 4 PARAMETERS OF THE EXPONENTIAL FITTING FUNCTIONS FOR TM POLARIZATION

Channel	a	b	R
1	0.2729	-1.04350	0.86466
2	0.3552	-1.38080	0.94315
3	0.38822	-1.48760	0.94874
4	0.3552	-1.38080	0.94315
5	0.2729	-1.04350	0.86466

3.3 Comparison of output power between TE and TM polarized input field

If we compare the output power of the MMI waveguide between TE and TM polarized input field, we can clearly observe that output power for TE polarization is higher than TM polarization, as shown in Fig. 10. This may be due to the lower attenuation and dispersion for TE polarization as we increase periodicity. In addition, the slight difference in MMI width between TE and TM polarization, implied from (4), may be another factor for the lower output power for TM polarization. The higher attenuation for TM polarization is observed even from the values of the *b* coefficient in Table 4, which have a greater absolute value than those in Table 3.

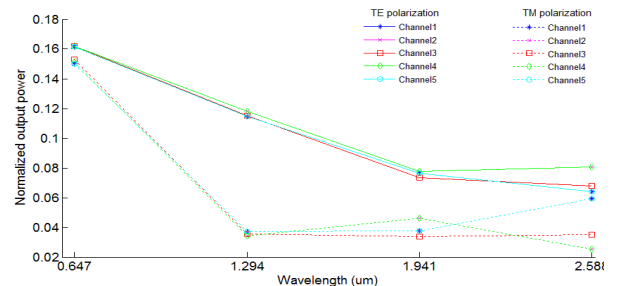


Fig. 10. TE and TM polarization output power for each channel

3.4 Excess loss and Power imbalance for TE and TM polarization

Practical applications such as optical fibre communication systems usually require optical circuits with low loss and balanced power splitting.. Here we calculate two of the commonly used performance parameters that are more specifically related to MMI devices, excess loss, $L_e(dB)$, and power imbalance, $L_b(dB)$ [5]. Excess loss is defined as the logarithmic difference between the sum of the powers in the output channels and the power in the input channel.

$$L_e(dB) = -10 \log_{10} (\sum_j P_j / P_{in}) \tag{5}$$

where P_j is the power in each output channel for $j = 1, 2, 3, \dots$, and P_{in} is the input power of the waveguide. In the previous paragraphs we showed that output power in MMI waveguides for both polarizations decreases exponentially with the increase of the wavelength. This implies that excess loss will increase with the increase of the wavelength for both polarizations. Table 5 shows the excess loss values for the four wavelengths considered in these simulations for TE and TM polarization.

TABLE 5 EXCESS LOSS FOR TE AND TM POLARIZATION

Wavelength (μm)	0.647	1.294	1.941	2.588
TE polarization Excess loss (dB)	0.922	2.362	4.187	4.327
TM polarization Excess loss (dB)	1.218	7.481	6.978	6.895

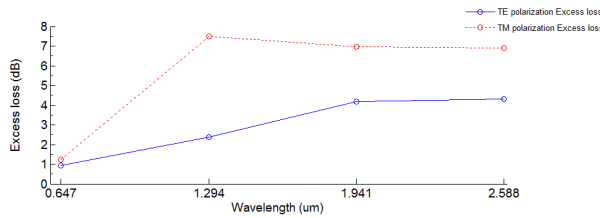


Fig. 11. Excess loss for TE and TM polarization vs. wavelength

Fig. 11. clearly shows that excess loss is greater for a TM polarized field compared to a TE polarized one. If a figure of 1 dB is accepted for the excess loss [7], we can infer from Table 5 that only a TE polarized field with a wavelength $\lambda = 0.647$ nm can be used with this waveguide for application purposes. Power imbalance, $L_b(dB)$, is defined as the logarithmic difference between two of the desired outputs.

$$L_b(dB) = -10\log_{10}(P_{d1}/P_{d2}) \tag{6}$$

Table 6 shows power imbalance for $\lambda = 0.647$ μm, for the 10 different channel pairs of the waveguide with 5 output channels that we simulated.

TABLE 6 POWER IMBALANCE FOR $\lambda = 0.647$ μm

Channel pair	TE polarization	TM polarization
	Power imbalance (dB)	
1-2	0.0201	0.0289
2-3	-0.0011	0.0555
3-4	0.0011	-0.0555
4-5	-0.0201	-0.0289
1-3	0.0189	0.0844
1-4	0.0201	0.0289
1-5	$1.620 \cdot 10^{-13}$	$-5.786 \cdot 10^{-14}$
2-4	$5.352 \cdot 10^{-14}$	$-2.893 \cdot 10^{-14}$
2-5	-0.0201	-0.0289
3-5	-0.0189	-0.0844

Table 6 shows that power imbalance for all channel pairs has relatively small values for both polarizations. This is especially emphasized for channel pairs 1-5 and 2-4 that are symmetrical in reference to channel 3. Therefore, the MMI waveguide in consideration is working as a good power splitter by offering almost equal power at each output channel. This characteristic makes it suitable to be used in the new design of the biosensor for splitting the input power.

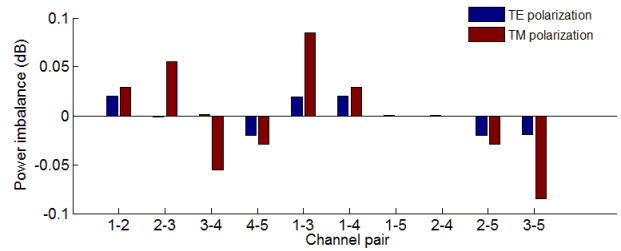


Fig. 12. Power imbalance for each output channel pair

3.5 Excess loss for the first period of replicas for different MMI lengths

Referring to equation (2), we have calculated the length of the MMI waveguide in order to take the first period of replicas for the wavelengths in consideration. Table 7 shows excess loss for these wavelengths and the respective MMI length.

3.5 Excess loss for the first period of replicas for different MMI lengths

Referring to (2), we have calculated the length of the MMI waveguide in order to take the first period of replicas for the wavelengths in consideration. Table 7 shows excess loss for these wavelengths and the respective MMI length.

TABLE 7 EXCESS LOSS FOR DIFFERENT MMI LENGTHS

Wavelength (μm)	0.647	1.294	1.941	2.588
L_{MMI} (mm)	13.91	6.955	4.637	3.478
	Excess loss (dB)			
TE polarization	0.922	1.011	1.548	1.638
TM polarization	1.218	1.508	0.481	2.873

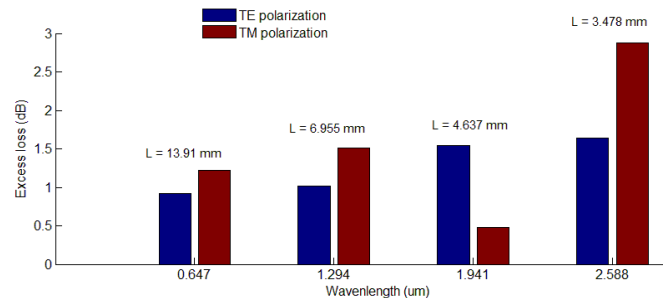


Fig. 13. Excess loss for 4 different wavelengths for first periodicity of replicas

Again the values show that excess loss is higher for TM polarization. Excess loss is under 1 dB at $\lambda = 647$ nm for TE polarization while for TM polarization excess loss is under 1 dB for $\lambda = 1.941$ μm.

4 SIMULATION OF MMI WAVEGUIDE WITH 10 OUTPUT CHANNELS

The parameters of this waveguide are the same with that shown in Fig. 4. except the fact that it has ten output channels. In this case the interdistance between output

channels will be $l_{int} = W_0/N = 150\mu m/10 = 15\mu m$. The wavelengths used in the simulations of this waveguide are:

1. $\lambda_1 = 0.3235 \mu m$
2. $\lambda_2 = 2\lambda_1 = 0.647 \mu m$
3. $\lambda_3 = 2\lambda_2 = 4\lambda_1 = 1.294 \mu m$

Table 8 shows the length of the MMI device for each wavelength and the respective excess loss.

TABLE 8 EXCESS LOSS FOR 3 DIFFERENT WAVELENGTHS FOR TE AND TM POLARIZATION

Wavelength (μm)	0.3235	0.647	1.294
L_{MMI} (mm)	13.91	6.955	3.477
Excess loss (dB)			
TE polarization	0.615	1.334	0.606
TM polarization	0.662	0.989	0.541

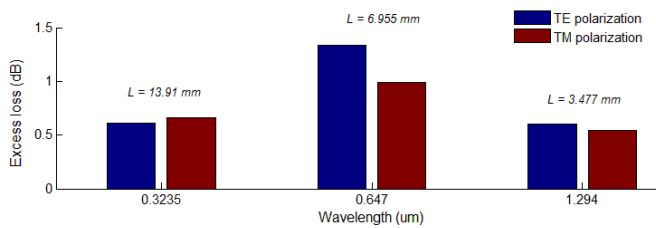


Fig. 14. Excess loss for 3 different wavelengths for TE and TM polarization

From the values in Table 8 we can infer that all the three wavelengths can be used for application purposes, if a figure of 1 dB is accepted for the excess loss [7].

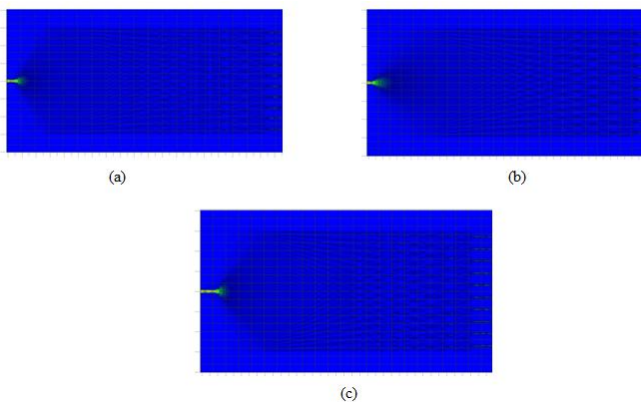


Fig. 15. Field distribution for a TE polarized field inside the MMI waveguide: a) $\lambda_1 = 0.3235 \mu m$, $L_{MMI} = 13.91$ mm b) $\lambda_2 = 0.647 \mu m$, $L_{MMI} = 6.955$ mm c) $\lambda_3 = 1.294 \mu m$, $L_{MMI} = 3.477$ mm

5 EXCESS LOSS COMPARISON BETWEEN TWO MMI WAVEGUIDES FOR TE AND TM POLARIZATION

Let us now compare excess loss between the two MMI waveguides that we have considered so far, with 5 and 10 output channels. The calculations are done for two different

wavelengths in order to take the first periodicity of the replicas in both cases. Table 9 shows the excess loss for TE and TM polarization for these two wavelengths, and the respective MMI length.

TABLE 9 EXCESS LOSS FOR TE AND TM POLARIZATION FOR TWO MMI WAVEGUIDES

Wavelength (μm)	0.647		1.294	
N	5	10	5	10
L_{MMI} (mm)	13.91	6.955	6.955	3.477
Excess loss (dB)				
TE polarization	0.922	1.334	1.011	0.606
TM polarization	1.218	0.989	1.508	0.541

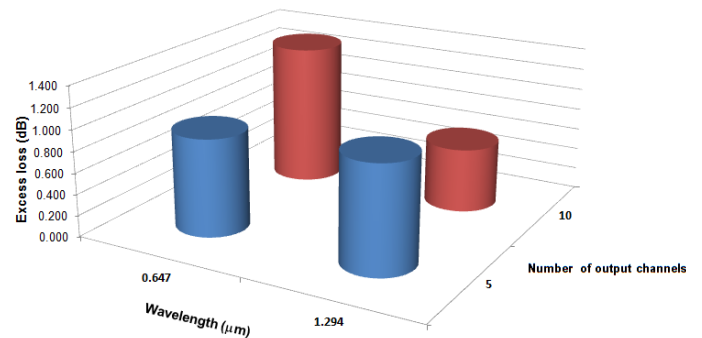


Fig. 16. Excess losses for TE polarization for the two MMI devices

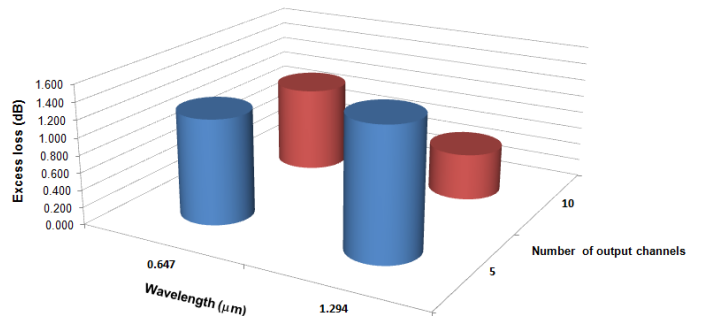


Fig. 17. Excess losses for TM polarization for the two MMI devices

From the values in Table 9 we can infer that excess loss remains almost the same for $\lambda = 647$ nm for both waveguides and polarizations, while for $\lambda = 1.294$ nm excess loss is two to three times higher for the waveguide with 5 output channels for both polarizations.

6 CONCLUSION

The MMI based sensor design presented in this paper is a novel approach towards a more compact biosensor and with a higher analysis throughput compared to the YI biosensor. By using the MMI effect the size of the biosensor will be reduced significantly and it will directly contribute to the reduction of its cost. This will create the possibility to increase the number of measuring channels and will improve their integration in micro-scale chips by making

them more portable. The evaluation of the excess loss and power imbalance by simulating the first MMI waveguide with OptiBPM software, showed that it offers the best performance as a power splitter by using a TE polarized profile input field with a wavelength of 647nm. To the best of our knowledge, MMI devices have never been investigated for sensing immune reactions, so this design is a novel contribution to the field of optical immunosensing.

Noordman, N. F. Hulst, and Th. J. Popma, "Optimization of LPCVD silicon oxynitride growth to large refractive index homogeneity and layer thickness uniformity", vol. 3099 of Proceedings of SPIE, pp. 257–268, Munich, Germany, June 1997.

REFERENCES

- [1] A. Ymeti, "Development of a Multichannel Integrated Young Interferometer Immunosensor," PhD dissertation, MESA+ Inst. for Nanotechnology, Univ. of Twente, Netherlands, 2004. (Thesis).
- [2] P. A. Besse, M. Bachmann, H. Melchior, L. B. Soldano, and M. K. Smit, "Optical Bandwidth and Fabrication Tolerances of Multimode Interference Couplers." vol. 12, pp. 1004-1009, Jun. 1994, doi: 10.1109/50.296191, *Journal of Lightwave Technology*.
- [3] H. P. Chan, S. Y. Cheng and P. S. Chung., "Novel design of low-loss wide-angle symmetric Y-branch waveguides." *Microwave and Optical Technology Letters*, Vol. 11, pp. 87–89, 5 Feb. 1996.
- [4] L. B. Soldano, and E. C. M. Pennings, "Optical Multi-Mode Interference Devices Based on Self-Imaging: Principles and Applications" , vol. 13, pp. 615-627, *Journal of Lightwave Technology*, Apr. 1995, ISSN: 0733-8724.
- [5] L. B. Soldano, F. B. Veerman, M. K. Smit, B. Verbeek, "Planar Monomode Optical Couplers Based on Multimode Interference Effects", vol. 10, pp. 1843-1850, doi: 10.1109/50.202837, *Journal of Lightwave Technology*..
- [6] R. M. Jenkins, R. W. J. Devereux, and J. M. Heaton "Waveguide beam splitters and recombiners based on multimode propagation phenomena.", vol.. 17, pp. 991-993, doi.: 10.1364/OL.17.000991 *Optics Letters*, 1992,
- [7] L. B. Soldano, M. Bachmann, P. A. Besse, and M. K. Smit, "Large Optical Bandwidth of InGaAsP/InP Multi-Mode Interference 3-dB Couplers" 6th *ECIO, Neufchatel, Switzerland*, Apr. 1993 (Conference Proceedings).
- [8] A. Ymeti, J. Greve, P. V. Lambeck, T. Wink, S. W. F. M. van Hövell, T. A. M. Beumer, R. R. Wijn, R. G. Heideman, V. Subramaniam, and J. S. Kanger, "Fast, ultrasensitive virus detection using a young interferometer sensor," vol.. 7, no. 2, pp. 394-397, *Nano Letters*, 2007
- [9] E. F. Schipper, R. P. H. Kooyman, R. G. Heideman, and J. Greve. "Feasibility of optical waveguide immunosensors for pesticide detection: physical aspects", Elsevier Science, Vol. 24, pp. 90-93. ISSN:1873-3077,1995, *Sensors and Actuators B: Chemical*
- [10] K. Wörhoff, P. V. Lambeck, H. Albers, O. F.